The Energy Transition's Impact on the Accumulated Average Efficiency of Large Hydrogenerators

Yannick Cyiza Karekezi, *Student Member, IEEE*, Thomas Øyvang, *Member, IEEE*, and Jonas Kristiansen Nøland, *Member, IEEE*

***Abstract*—The energy transition is aimed to take advantage of the operational flexibility of hydropower to extend the integration of intermittent renewable sources. Consequently, the hydrogenerators will have to operate in regimes far away from their designed best-point operation. In order to accurately assess the impact, this paper presents a useful approach to determine the overall operating efficiency of synchronous generators under intermittent operation. An accumulated average efficiency (AAE) model is proposed and compared against an alternative approach; the weighted average efficiency (WAE) model. It is found that the WAE approach produces unrealistic low efficiencies when the generator operates in synchronous condenser mode (SCM) for long periods. In general, the AAE supersedes the WAE for all the different load distributions that were investigated. This was further illustrated by a worked example and by constructing more complex load distributions. A load distribution dominated by SCM yields a difference as high as $33.18\,\%$, while an even distribution deviates $1.43\,\%$ in their respective efficiencies. Finally, a yearly on-site measurement of our studied 103 MVA generator's concentrated load distribution revealed a discrepancy of $0.67\,\%$, which is a significant deviation considering what the operating regime would mean in terms of economic implications.**

***Index Terms*—Synchronous machines, saturation modeling, efficiency modeling, loss measurement.**

NOMENCLATURE

Δt_i	Discrete time interval for a load point, $[h]$ or $[s]$
δ	Rotor loading angle, $[rad]$ or $[^\circ]$
η	Generator's operation point efficiency, $[pu]$ or $[\%]$
η_a	Accumulated average efficiency (AAE), $[pu]$ or $[\%]$
η_n	Generator's nominal efficiency, $[pu]$ or $[\%]$
η_w	Weighted average efficiency (WAE), $[pu]$ or $[\%]$
$\mathcal{E}_g$	Total fictive induced generator voltage, $[pu]$ or $[V]$
$\mathcal{E}_p$	Induced voltage behind potier reactance, $[pu]$ or $[V]$
$\overline{P}$	Mean power, $[pu]$ or $[kW]$
$\overline{P}_{loss}$	Mean power loss, $[pu]$ or $[kW]$
θ	Angle behind the potier reactance, $[rad]$ or $[^\circ]$
φ	Power factor angle, $[rad]$ or $[^\circ]$
A_i	Weighting factor for an operation point, $[pu]$ or $[\%]$
b_v	Slope constant of the generator's air gap line curve
C_m	Saturation constant for the generator's saturation curve
E	Generator's accumulated energy production, $[GWh]$
E_{loss}	Generator's accumulated energy losses, $[GWh]$
I_a	Stator armature current, $[pu]$ or $[A]$
I_f	Rotor field current, $[pu]$ or $[A]$
k	Slope constant for approximating the generator' saturation curve in the air gap line region
m	Saturation curve's exponential constant
P	Generator's active power, $[pu]$ or $[MW]$
P_a	Stator armature winding resistive loss, $[pu]$ or $[kW]$
P_{be}	Bearing loss, $[pu]$ or $[kW]$
P_{br}	Rotor brush loss, $[pu]$ or $[kW]$
P_c	Stator armature iron core loss, $[pu]$ or $[kW]$
P_{ex}	Excitation system loss, $[pu]$ or $[kW]$
P_f	Rotor field winding resistive loss, $[pu]$ or $[kW]$
P_{loss}	Generator's total losses, $[pu]$ or $[kW]$
P_s	Stator stray load loss, $[pu]$ or $[kW]$
P_{wf}	Windage and friction loss, $[pu]$ or $[kW]$
Q	Generator's reactive power, $[pu]$ or $[MVAr]$
R_a	Stator armature resistance, $[pu]$ or $[\Omega]$
S	Generator's apparent power, $[pu]$ or $[MVA]$
U_a	Stator armature terminal voltage, $[pu]$ or $[V]$
X_d	Direct axis synchronous reactance, $[pu]$ or $[\Omega]$
X_p	Potier reactance, $[pu]$ or $[\Omega]$
X_q	Quadrature axis synchronous reactance, $[pu]$ or $[\Omega]$

Manuscript received 19 October 2021; accepted 7 March 2022. Date of publication 11 March 2022; date of current version 22 August 2022. This work was supported by the Research Council of Norway (RCN) under Grant 326673 (SysOpt Project). Paper no. TEC-01139-2021. *(Corresponding author: Yannick Cyiza Karekezi.)*

Yannick Cyiza Karekezi and Jonas Kristiansen Nøland are with the Norwegian University of Science and Technology (NTNU), 7491 Trondheim, Norway, and also with the University of South-Eastern Norway (USN), 3918 Porsgrunn, Norway (e-mail: yannick.c.karekezi@ntnu.no; jonas.k.noland@ntnu.no).

Thomas Øyvang is with the University of South-Eastern Norway (USN), 3918 Porsgrunn, Norway (e-mail: thomas.oyvang@usn.no).

Color versions of one or more figures in this article are available at https://doi.org/10.1109/TEC.2022.3158566.

Digital Object Identifier 10.1109/TEC.2022.3158566

I. INTRODUCTION

OVER the last decade, the load cycling intervals of large hydropower plants have changed fundamentally from rated conditions to a diverse set of operating points. As a result of a significant integration of intermittent renewable energy sources (RES) to the grid, the classical generators have responded more often to dispatch the fluctuations in both voltage and power [1]–[3]. These operating regimes bring new economic costs into consideration, as the efficiency now becomes a significant differentiator. By convention, the nominal efficiency is usually taken for granted.

This paper's primary focus is how the energy transition affects the hydrogenerator units in terms of a more flexible operational regime. Future operating regimes imply frequent step changes

in active and reactive power production, and several start-stop cycles during the day and week [4]–[7], depending on the RES's weather pattern. It also implies running the generators in synchronous condenser mode (SCM), providing intermittent power reserves, buffers, and rotating inertia. Currently, there are few concrete plans from the US and European governments to reconstruct the present grid topology to adapt for a full-scale energy transition. In essence, it implies that the bulk power plants must handle the increasing volatility of the power grid when alternative large-scale energy storage solutions are not readily available. It is, therefore, a desire to design robust hydrogenerators for the future, taking their operational burden and the potential load fluctuations into account. Most of the generators today are not designed for these kinds of operational regimes as they are conventionally specified for a constant duty mode, and a nominal operating point [8]. Historically, the synchronous machine has operated in load points limited and concentrated around a relatively small region of the capability diagram. The reactive power has been varying slightly around a unity power factor, with reactive power generation dominating. In the future, this concentrated distribution is projected to be transformed into a more evenly distributed distribution pushing closer to the boundaries of the capability diagram. This effect is highlighted in [5]–[7], depicting changes as a result of the German "Energiwende." In addition, the capability diagram's maximum reactive limits might be extended further for extra reactive power reserves during shorter periods to provide enhanced grid voltage security [9]. Moreover, in periods of excess water, extra frequency support can be provided at peak hours if allowing an overloaded active power capability [10].

The ever-increasing introduction of RES results is intensified when hydropower is connected to larger geographical regions [11]. The increasing prevalence of these kinds of operational regimes requests the need for calculation models that can accurately quantify the overall impact for hydrogenerators [7], in addition to the operational burden at the turbine-side as well [12], [13]. The calculation model weighted average efficiency (WAE) offers a viable solution to quantify the RES' impact on hydro generators [1]–[3]. The computational scheme is a sampling average approximation approach to obtain the overall operating efficiency of generators varying over different loading conditions during a finite time period. However, the WAE has one primary weakness; it weights the efficiency for one loading point at a time and not the accumulation of the loading points. This means that if the generator is operated purely as a synchronous condenser (i.e., $P = 0$ pu) for a long time, one can get a large dataset of samples of zero efficiencies in the summation of average efficiencies. This reduces the WAE considerably.

This paper presents the concept of accumulated average efficiency (AAE) as a new and useful method to compute the mean efficiency of synchronous generators when they frequently vary their operating conditions. An illustration of the concept is depicted in Fig. 1, but further described in Section III. The method is compatible with both exact load points or load-grid distributions clustered in discrete points, as depicted in Fig. 2. The proposed AAE approach will be compared against the already established WAE [1]–[3].

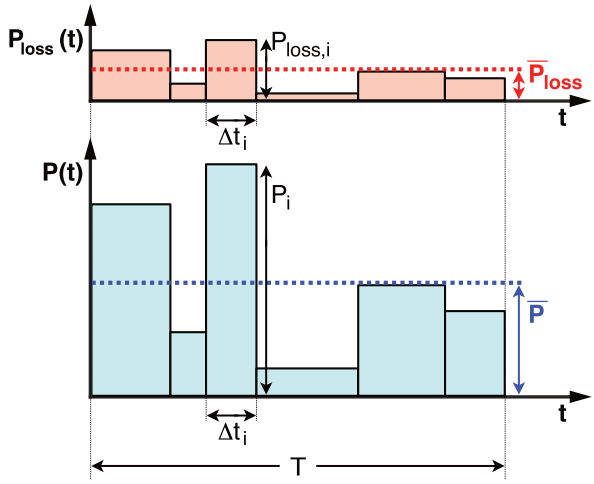

Fig. 1. Generic load cycling sequence for accumulation of the generator's energy loss (E_{loss}) and energy generation (E) over time formulated by discrete time intervals. E_{loss} is equal to the sum of all red areas, while E is the sum of all blue areas. The mean power loss ($\overline{P}_{loss} = E_{loss}/T$) and the mean power generation ($\overline{P} = E/T$) are also indicated.

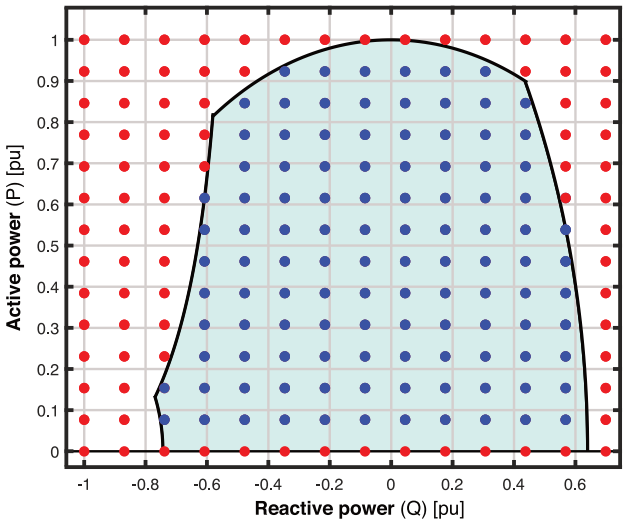

Fig. 2. Example of 110 blue uniformly distributed load points inside the capability diagram for the 103 MVA hydrogenerator considered in this paper. Red points are outside of the capability diagram.

In order to accurately predict the needed field current during different load operations, a different saturation modeling approach is utilized, taken as an alternative to what has already been proposed by Bortoni *et al.* for efficiency modeling [1]. Our calculations, simulations, and post-processing of measurements are all conducted in the MATLAB numerical environment. In order to confirm the predictions made by the efficiency model, on-site efficiency recordings were done at different load operations to ensure that the model could predict the efficiency for the major portions of the capability diagram. This enabled us also to make artificial load distributions to predict the implications of the energy transition's rapid increase in RES. The peculiar case of SCM-dominated operation was considered as the worst case. Moreover, real-world production data covering a whole year for

the considered hydrogenerator was post-processed to analyze the implications of the present-day load operations.

The paper is organized as follows. Section II reviews the power loss modeling and formulates the segregation of loss to be compatible with the proposed AAE. Then, in Sections III and IV, the proposed efficiency and saturation modeling approaches are described. Finally, Section V presents the main results from our handpicked case studies before Section VI concludes our findings.

II. Power Loss Modeling

This section briefly presents the loss modeling employed in this paper. For clarity, the nomenclature describes all the variables from the paper's beginning. The segregation of the loss components is needed for the efficiency modeling formulation but is independent of the chosen approach. Its general formulation has already been well described in [1]. Differently from the work of Bortoni *et al.* [1] is the explicit expression of the total losses (P_{loss}) to make the formulation compatible with our proposed AAE approach. Moreover, this paper also expresses a compressed formulation of the loss modeling in (2)–(5), merging the armature and strayload losses [14], and bringing the field winding and brush losses together. Moreover, the exciter loss is considered as directly proportional to the field current [15]. As usual, the bearing, windage, and friction losses appear as constant loss components. In addition, the iron core loss [16] is assumed as a constant since the armature voltage (U_a) is kept close to 1 pu, even though the flux angle can have a minor effect. The grid voltage is constrained to be between 0.95 and $1.05\,\mathrm{pu}$ in many grid codes [17], [18], implying that P_c will vary -9.75 % to +10.25 % from its base value. Hereafter, P_c is considered as a constant value, assuming $U_a = 1\,\mathrm{pu}$. This also implies that the per-unit armature current can be approximated as

$$I_a = \frac{\sqrt{P^2+Q^2}}{U_a} \approx \sqrt{P^2+Q^2}. \tag{1}$$

The field current (I_f) prediction is less straightforward and is separately described in Section IV.

The rated quantities of the active power losses are tagged with "*". Moreover, "*" is also used to indicate the nominal values of the armature current (I_a^*) and the field current (I_f^*), respectively. The load-dependent equations and assumptions for the iron core and excitation losses are not explicitly included in this manuscript but details can be found in [1].

$$P_a + P_s = (P_a^* + P_s^*)\left(\frac{I_a}{I_a^*}\right)^2 \tag{2}$$

$$P_f + P_{br} = (P_f^* + P_{br}^*)\left(\frac{I_f}{I_f^*}\right)^2 \tag{3}$$

$$P_{loss} = P_a + P_s + P_c + P_f + P_{br} + P_{ex} + P_{be} + P_{wf} \tag{4}$$

$$\eta = \frac{P}{P + P_{loss}} \tag{5}$$

(2)–(5) need to be evaluated for an exact load load operation point, e.g., $0.9\,\mathrm{pu}$ active power and $0.436\,\mathrm{pu}$ reactive power, which is the rated load point. In reality, all possible operating points are continuous. This means that the power does not jump from one power level to another. Fig. 1 presents the continuous power as time interval for specific load points. This is taken as an approximation of the continuous power, where power-ramping profiles are neglected. The same time intervals can also be visually represented in a P-Q diagram, where collections of the measured load points are clustered into discrete load points with a given probability of occurrence ($\frac{duration}{totaltime}$) using a 2D histogram [1]. In Fig. 2, an example of these discrete load points is defined in a grid structure inside the capability diagram. In a real case study, each discrete points' probability is determined by its proximity to actual measured load points. Therefore one can determine the probability ($\frac{duration}{totaltime}$) for the predefined load points based on the density of the measured load points and their duration recorded around these clustered points. Moreover, the red points outside the indicated capability diagram violate the machine's capacity limits and are therefore set to zero probability. A discrete point with high probability reveals that a large number of measured machine loading intervals occur in its proximity.

The probability of the occurrence for a particular load-interval can be understood from Fig. 1, where

$$A_i = \frac{\Delta t_i}{T}. \tag{6}$$

III. Efficiency Modeling

The calculation of the efficiency of several discrete points can then be used to obtain non-concentric curves that map the studied machine's efficiency characteristics at different load operations. This section takes our adapted power loss modeling on board to formulate a modeling approach for the overall operating efficiency. First, the challenges with the alternative WAE are presented before the proposed AAE is derived. It is worth noting that the basics of the WAE have already been well explored and studied in [1].

A. Weighted Average Efficiency (WAE)

The main obstacle with the WAE formulation lies in the efficiency definition, which has severe consequences for certain operational regimes such as the synchronous condenser mode (SCM) of operation. In the WAE formulation, the efficiency is calculated for every operating point and multiplied with its corresponding weight, where all weighted efficiencies are finally summed up to an average efficiency. The WAE can be expressed in the continuous time frame using (7), which is further explained in [1]. The WAE in the finite time intervals can be expressed using (8), where the efficiency of different operating points is weighted depending on their time duration over a period T. Alternatively, including its respective index (i) for finite time intervals, the WAE could be formulated with (9).

$$\eta_w = \frac{1}{T}\int_0^T \eta(t)dt, \tag{7}$$

$$\eta_w = \sum_{i=1}^{n} \eta_i \frac{\Delta t_i}{T} = \sum_{i=1}^{n} \eta_i A_i = \eta_1 A_1 + \eta_2 A_2 + \cdots + \eta_n A_n \tag{8}$$

$$\eta_w = \sum_{i=1}^{n} \frac{P_i}{P_i + P_{loss,i}} A_i \tag{9}$$

From the expressions above, the WAE is seen to be directly proportional to the efficiency of the weighted load points. I.e., if one-third of the given dataset's efficiency is zero (e.g., under SCM operation), then the WAE gets reduced by $\frac{1}{3}$. Consequently, it also means that the WAE can not be higher than 66 % when the generator operates $\frac{1}{3}$ of its running time as a synchronous condenser. This can be illustrated by inserting (10) as an element into (8).

$$\eta_{scm} = \frac{P_{scm}}{P_{scm} + P_{scm,loss}} = \frac{0}{0 + P_{scm,loss}} = 0\,\% \tag{10}$$

(10) clearly shows that there is an unclear representation of the inefficiency as the losses are not accounted for when the generator runs in SCM of operation. If one imagines that the (10) occurs $\frac{1}{3}$ of the time during its yearly operation, it would mean that one has not accurately quantified the actual machine losses during $\frac{1}{3}$ of the generators' operating time.

Let us consider a simple example where the generator operates in two distinct operating points over a full period, where the generator operates at rated conditions $\frac{2}{3}$ of its time, Δt (i.e., $\frac{\Delta t}{T} = \frac{2}{3}$), with efficiency η_n, and as a synchronous condenser during $\frac{1}{3}$ of its operating time, $T - \Delta t$ (i.e., $1 - \frac{\Delta t}{T} = \frac{1}{3}$). Insertion of these conditions into (7) yields that the WAE is expressed as

$$\eta_{\mathrm{w}} = \frac{1}{T}\left(\eta_n \cdot \underbrace{\Delta t}_{=\frac{2}{3}T} + \underbrace{\eta_{scm}}_{=0} \cdot (T - \Delta t)\right) = \left(\frac{2}{3}\right)\eta_n, \tag{11}$$

yielding a WAE two-thirds of the nominal efficiency.

B. Accumulated Average Efficiency (AAE)

The proposed AAE follows an entirely different calculation procedure, as illustrated in Fig. 1. The total accumulated energy generation (E) and energy losses (E_{loss}) are the basis for the AAE, as expressed in (12). This approach merely takes the accumulated E and E_{loss} into account, which minimizes the influence of very low efficiencies under SCM operation.

$$\eta_a = \frac{E}{E + E_{loss}} = \frac{\int_0^T P(t)dt}{\int_0^T P(t)dt + \int_0^T P_{loss}(t)dt} \tag{12}$$

In the finite time formulation, the AAE first starts by computing the actual active power losses ($P_{loss,i}$) for each the discrete time interval (Δt_i) given by index i for a given load point P_i. Then, the sum of all the actual power elements (P_i and $P_{loss,i}$) are multiplied individually by the time duration (Δt_i) to obtain average values or expected values in terms of accumulated energy (E and E_{loss}), as formulated in (13) and (14), where the total time (T) is given in (15).

$$E_{loss} = \sum_{i}^{n} P_{loss,i}\Delta t_i = P_{loss,1}\Delta t_1 + P_{loss,2}\Delta t_2 + \cdots + P_{loss,n}\Delta t_n \tag{13}$$

$$E = \sum_{i}^{n} P_i \Delta t_i = P_1\Delta t_1 + P_2\Delta t_2 + \cdots + P_n\Delta t_n \tag{14}$$

$$T = \sum_{i}^{n} \Delta t_i = \Delta t_1 + \Delta t_2 + \cdots \Delta t_n \tag{15}$$

In order to convert the expressions into weighted sums, (13) and (14) are modified into the mean power generation ($\overline{P}$) and the mean power loss ($\overline{P}_{loss}$) in (16) and (17), respectively.

$$\overline{P} = \frac{E}{T} = \sum_{i}^{n} P_i A_i = P_1 A_1 + P_2 A_2 + \cdots P_n A_n \tag{16}$$

$$\overline{P}_{loss} = \frac{E_{loss}}{T} = \sum_{i}^{n} P_{loss,i} A_i = P_{loss,1} A_1 + P_{loss,2} A_2 + \cdots P_{loss,n} A_n \tag{17}$$

The normalization ensures that the sum of the weights (A_i) is equal to unity, yielding

$$1 = \sum_{i}^{n} \frac{\Delta t_i}{T} = \sum_{i}^{n} A_i = A_1 + A_2 + \cdots A_n. \tag{18}$$

The time-based and the weight-based formulations of the AAE are provided in (19) and (20), respectively.

$$\eta_a = \frac{E}{E + E_{loss}} = \frac{\sum_i^n P_i \Delta t_i}{\sum_i^n P_i \Delta t_i + \sum_i^n P_{loss,i}\Delta t_i} \tag{19}$$

$$\eta_a = \frac{\overline{P}}{\overline{P} + \overline{P}_{loss}} = \frac{\sum_i^n P_i A_i}{\sum_i^n (P_i + P_{loss,i}) A_i} \tag{20}$$

IV. Magnetic Saturation Modeling

As mentioned above, the generator loading condition impacts the field current (I_f), where loss components apply, as expressed in (3). Consequently, the machine's magnetic saturation plays a role in determining the losses and the efficiency accurately. In other words, this means that one cannot assume that the generator's field current I_f is directly proportional to the induced voltage $\mathcal{E}_g$, as in the linear region.

The open-circuit characteristics (OCC) are given by the manufacturer's datasheet and are in line with the measurements presented in Fig. 3, for the particular machine studied in this paper. A mathematical relation is set up to fit the measured data points of the saturation curve. The OCC is converted to a per-unit system, where the field current (I_f) is scaled by the nominal field current of the air gap line characteristics. For this particular case, the $I_{f0,base}$ is 525.15 A. The rated current (I_f) given in Table II will then have a normalized value of 2.028 pu, with a physical value of 1065 A.

A wide range of methods is applicable to express the OCC in mathematical terms. Our handpicked (22) that fits the data

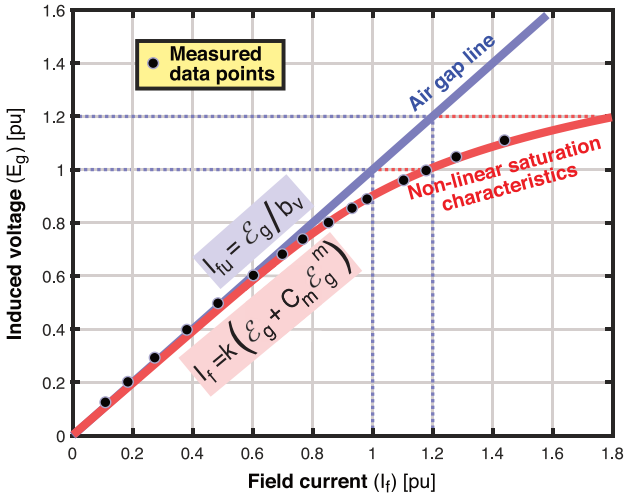

Fig. 3. Per-unit saturation curve of the 103 MVA synchronous machine aligned with measured operating points measured at no-load conditions and rated speed of 500 rpm. This machine is considered as a case study in Section V. The air gap line curve and the non-linear staturation characteristics refers to (21) and (22), respectively (coefficients are given in Table I). The base field current and line voltage is 525.15 A and 11 kV.

TABLE I
COEFFICIENTS USED FOR THE FITTING (21) AND (22) IN FIG. 3

Symbols	b_v	C_m	$\mathcal{E}_g$	m	k
Values	1	0.160	0 - 1.8	7	1.0308

TABLE II
KEY QUANTITIES OF THE STUDIED HYDROGENERATOR

Symbol	Description	Value
S_b	Base apparent power	103 MVA
cos (φ)	Power factor	0.90
η_n	Measured rated efficiency	98.834 %
U_t	Nominal armature voltage	11 kV
I_t	Nominal armature current	5406 A
I_f	Rated field current	1065 A
f	Nominal frequency	50 Hz
p	Number of poles	12
n	Nominal speed	500 rpm

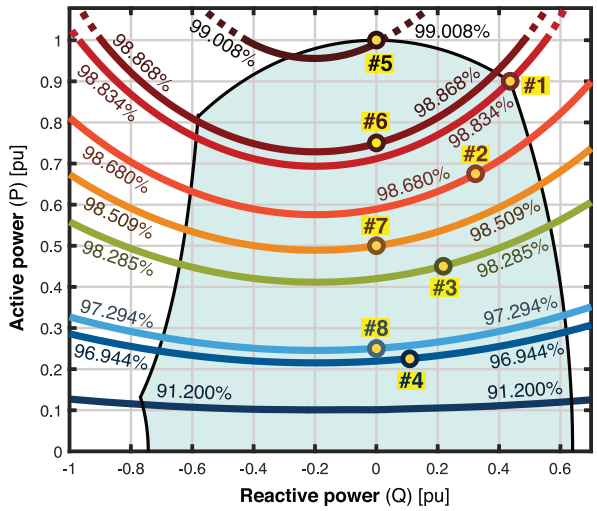

Fig. 4. Mapping of the calculated iso-efficiency curves of the capability diagram of the 103 MVA synchronous machine, and assessed against eight measured operating points (referring to Table IV). S_{max} =1 pu. The left side of the capability diagram's boundary has 20 % stability margin from the theoretical stability limit.

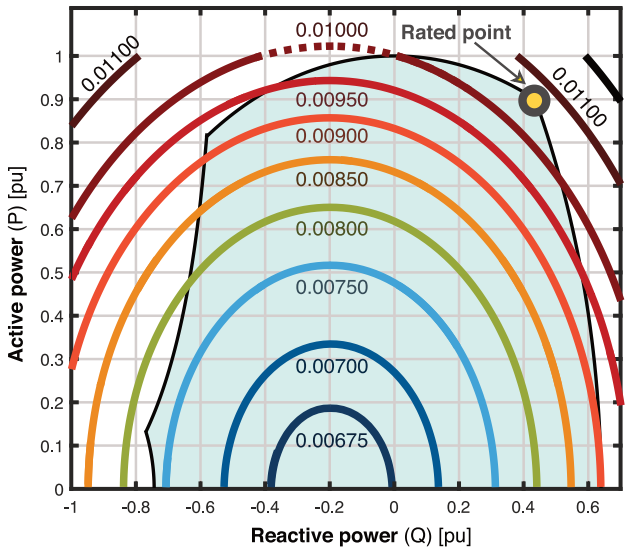

Fig. 5. Mapping of the calculated power loss contours over the capability diagram of the 103 MVA synchronous machine in per unit with 103 MVA as the power base.

has its coefficients presented in Table I. Beneficially, only two values need to be tuned, C_m and k, that are arbitrary constants. The function stems from the generator fundamentals presented by Machowski [19], based on earlier works on saturation. Our extension is using the proposed constant k in this paper, extending the classical formulation to make it compatible with the air gap line linear region, predicted by (21). As a result, (22) needs no arbitrary saturation threshold as it can approximate the OCC of the linear region and the saturation region, simultaneously. Usually, the slope of the air gap line is equal to 1 pu, which is formulated in (21), if b_v is set to 1 pu.

$$I_{fu} = \frac{\mathcal{E}_g}{b_v} \tag{21}$$

$$I_f = k(\mathcal{E}_g + C_m \mathcal{E}_g^m) \tag{22}$$

The procedure is as follows. First, the coefficient m is selected as either 7 or 9. Then, the two other constants, k, and C_m are found from a fitting procedure to obtain the red curve in Fig. 3. An alternative approach is found in Bortoni *et al.* [1] that uses a fourth-order polynomial regression of the non-linear saturation characteristic to provide five polynomial coefficients. This method has a high accuracy for expressing the saturation curve but needs more arbitrary valued coefficients and a separate equation for the air gap line below a certain threshold. This paper takes a different path, where (22) applies to the whole domain of the OCC, making it computationally user-friendly, less sensitive to parameter values and arbitrary thresholds. Based on the Potier method, obtaining I_f is formulated differently, as given in (23).

$$I_f = \frac{\mathcal{E}_g - \mathcal{E}_p}{b_v} + k(\mathcal{E}_p + C_m \mathcal{E}_p^n) \tag{23}$$

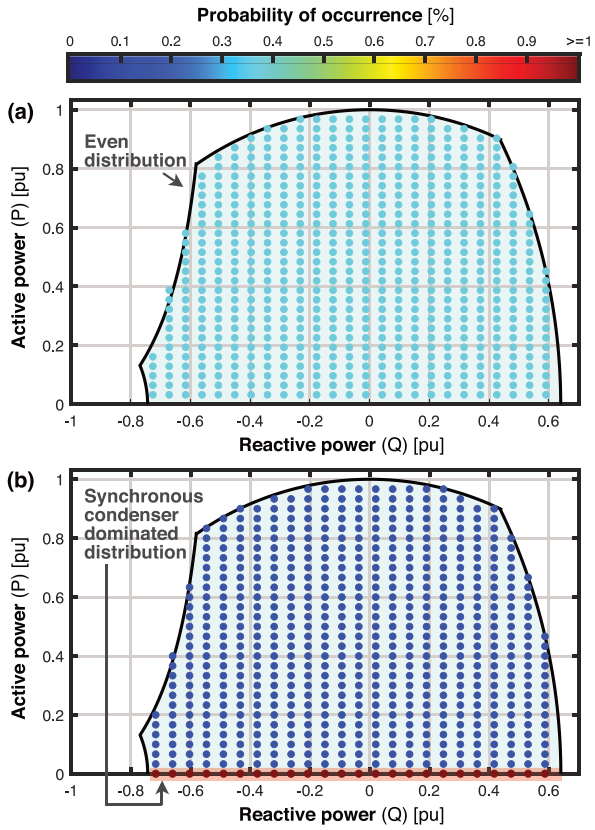

Fig. 6. Two-dimensional histograms for the probability of occurrence of different intermittent load operations that are artificially made as worst-case scenarios, i.e., a uniform load distribution (641 elements) and a synchronous condenser dominated distribution (623 elements), respectively. The theoretical limits go beyond the changes reported in [1] and [7], to expand on the consequences of RES, which are further summarized in Table IX).

Both $\mathcal{E}_g$ and $\mathcal{E}_p$ are found from I_a in (1) and the power factor angle given by $\varphi = \tan^{-1}(Q/P)$. $\mathcal{E}_g$ is the fictive induced voltage behind X_d and X_q, while $\mathcal{E}_p$ lies behind X_p, as explained in [20], [21], and further applied in [1]. However, before obtaining $\mathcal{E}_g$ and $\mathcal{E}_p$, their respective voltage angles, δ and θ, are often estimated, if not an all-in-one complex formulation is utilized. The saturation modeling is further validated under full-load condition in Section V-A, extending the preliminary no-load verification of Fig. 3.

V. Case Study and Main Results

This section presents the case study and the main results used to emphasize the paper's contributions, which is the impact the energy transition has on the hydro-generator facilities. In Table II, the key quantities describing a 103 MVA Norwegian hydro generator is listed. There is also a list of designed and measured machine characteristics in Table III. Finally, the determination of losses and the corresponding efficiency was conducted according to the IEEE 115, 7.2.4 method 4 [20] as three separate off-grid heat-run tests: (a) open, (b) short circuit, and (c) zero excitation, where some of the results are listed in Table IV. The same generator facility has been thermally investigated in an earlier six-hour heat run test (grid-connected) to identify rated load temperature rises [22]. Alternatively, an infrared thermal imaging technique could have been employed [23].

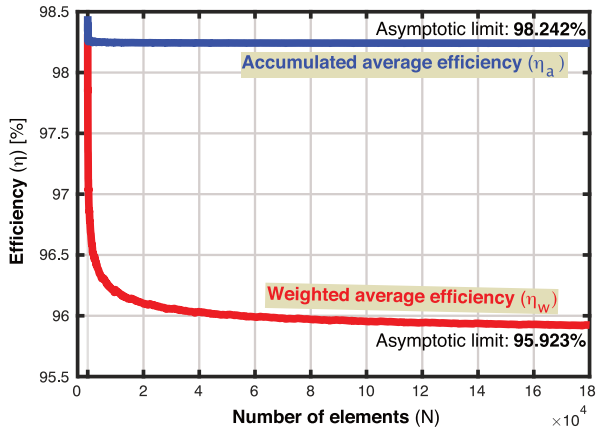

Fig. 7. Weighted average efficiency (η_w) and accumulated average efficiency (η_a) as a function of number of elements for even load distribution over the capability diagram of the 103 MVA hydrogenerator, referring to Fig. 2.

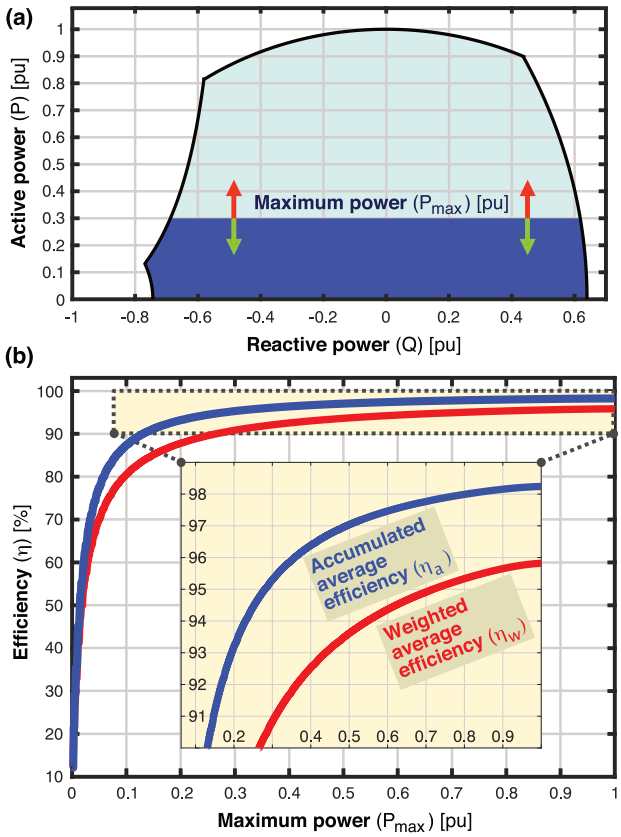

Fig. 8. Weighted average efficiency (η_w) and accumulated average efficiency (η_a) as a function of maximum power for even load distribution over the capability diagram of the 103 MVA synchronous machine. **a)** Definition of the maximum power (P_{max}) with the dark blue area covering the evenly distributed load points. **b)** Efficiencies (η_w and η_a) plotted in terms of P_{max}, converging toward the values presented in Table VIII as P_{max} approaches 1 pu. The maximum number of elements (N) where 171075.

TABLE III
STUDIED HYDROGENERATOR'S PARAMETER VALUES

Symbol	Description	Designed	Measured
R_a	Armature resistance	0.002 pu	
X_d	Direct axis reactance	1.087 pu	1.059 pu
X_q	Quadrature axis reactance	0.676 pu	
X_p	Potier reactance	0.144 pu	0.141 pu
X_l	Leakage axis reactance	0.080 pu	

A. Experimental Validation of Efficiencies and Saturation

Eight on-site measurements verifying the loss model at different operations are documented in Table IV. An iso-efficiency map of our model was then plotted together with the measured efficiencies in Fig. 4. The calculated non-concentric curves from (2)-(5) show a good agreement with the measured operating points of Table IV, as indicated in Fig. 4. From the outputs, the power loss contours are also plotted (in Fig. 5). This additional map is needed to conduct the proposed AAE, which is different from the alternative WAE. It was found that the most sensitive loss contribution was the saturation model, which predicts I_f and relates to the exciter and rotor related losses. In Table V, the accuracy of this model was assessed against the measurements, revealing a worst-case deviation of $1.79\,\%$, occurring in measurement number $\#5$.

B. Worked Example Assessing AAE Against WAE

The method which provided the the post-processed iso-curves presented in the last subsection will now be used as a basis to compare the proposed AAE against the alternative WAE in a worked example. For simplicity, six distinct operating points are considered throughout a whole year of operation. The hand-picked load points are given in Table VI, specifying their output metrics. Finally, the individual load point's outputs are used to compare the AAE against the WAE in Table VII. Notice that this is a simple example to demonstrate the core principles of the calculation models and not actual yearly production. I.e., the results presented are used to offer valuable insight into what differentiates the calculation models. The analytical calculation presented can also be easily reproduced by hand, which ensures the integrity of our work. The WEA is given by (8) and calculated using (24).

$$\eta_w = \eta_1 A_1 + \eta_2 A_2 + \eta_3 A_3 + \eta_4 A_4 + \eta_5 A_5 + \eta_6 A_6$$

$$= \frac{0}{6} + \frac{0}{6} + \frac{98.509}{6} + \frac{98.215}{6} + \frac{99.011}{6} + \frac{98.886}{6} = 65.77\,\% \tag{24}$$

Moreover, the AAE is given by (19). Herein, the mean power ($\overline{P}$) is inserted to be $0.5\,\text{pu}$ from (16) and the mean power loss ($\overline{P}_{loss}$) is found to be $0.00887\,\text{pu}$ from (17). Using (20), the AAE efficiency is then found to be

$$\eta_a = \frac{\overline{P}}{\overline{P} + \overline{P}_{loss}} = \frac{0.5}{0.5 + 0.00887} = 98.256\,\%. \tag{25}$$

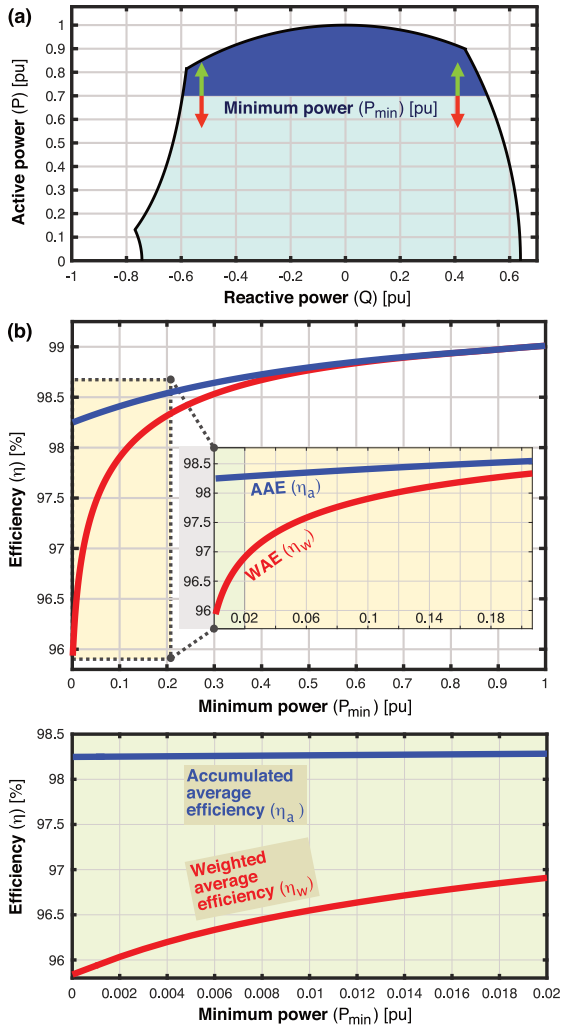

Fig. 9. Weighted average efficiency (η_w) and accumulated average efficiency (η_a) as a function of minimum power for even load distribution over the capability diagram of the 103 MVA synchronous machine. **a)** Definition of the minimum power (P_{min}) with the dark blue area covering the evenly distributed load points. **b)** Efficiencies (η_w and η_a) plotted in terms of P_{min}, converging toward the values presented in Table VIII as P_{min} approaches $0\,\text{pu}$. The maximum number of elements (N) where 171075.

In general, it can be seen that the efficiency difference between η_a and the alternative η_w is $33.18\,\%$ for this primitive example. The huge deviation is explained by the worked example's subsequent long periods operating at $P = 0\,\text{pu}$, i.e., at zero efficiencies ($\eta = 0\,\%$). It is far from surprising, as the WAE is reduced proportionally to the amount of time the generator operates in SCM, as already predicted by (11). The example provides preliminary theoretical support for the superiority of the proposed AAE approach. The same approaches will now be analyzed with more complex datasets and measured data in the next subsections.

C. Sensitivity of Even Load Distribution's Number of Elements

Expanding on the worked example, Fig. 6 shows two more complex load distributions that are more computationally demanding. The first one (a) is the evenly distributed case, and

TABLE IV
ON-SITE MEASURED QUANTITIES AT EIGHT DISTINCT LOAD POINTS FOR THE 103 MVA MACHINE USED FOR THE EFFICIENCY ANALYSIS IN FIG. 5, WHERE THE NUMBER, CORRESPONDING LOAD POINT AND EFFICIENCY IS HIGHLIGHTED

Output	**#1**	**#2**	**#3**	**#4**	**#5**	**#6**	**#7**	**#8**
S	1.000 pu	0.750 pu	0.500 pu	0.250 pu	1.000 pu	0.750 pu	0.500 pu	0.250 pu
$\cos(\varphi)$	0.900	0.900	0.900	0.900	1.000	1.000	1.000	1.000
P	0.900 pu	0.675 pu	0.450 pu	0.225 pu	1.000 pu	0.750 pu	0.500 pu	0.250 pu
Q	0.436 pu	0.327 pu	0.218 pu	0.109 pu	0.000 pu	0.000 pu	0.000 pu	0.000 pu
I_a	5406.1 A	4054.6 A	2703.0 A	1351.5 A	5406.1 A	4054.6 A	2703.0 A	1351.5 A
I_f	1065.00 A	936.12 A	816.18 A	711.38 A	873.17 A	776.61 A	698.70 A	646.84 A
P_f	173.65 kW	133.66 kW	101.61 kW	77.19 kW	116.29 kW	91.99 kW	74.48 kW	63.81 kW
P_{ex}	15.88 kW	13.02 kW	10.72 kW	8.87 kW	11.65 kW	9.92 kW	8.68 kW	7.92 kW
P_{br}	2.13 kW	1.87 kW	1.63 kW	1.42 kW	1.75 kW	1.55 kW	1.40 kW	1.29 kW
P_a	187.46 kW	105.45 kW	46.86 kW	11.72 kW	187.46 kW	105.45 kW	46.86 kW	11.72 kW
P_s	89.16 kW	50.15 kW	22.30 kW	5.57 kW	89.16 kW	50.15 kW	22.30 kW	5.57 kW
P_c	211.92 kW	211.92 kW	211.92 kW	211.92 kW	211.92 kW	211.92 kW	211.92 kW	211.92 kW
P_{be}	240.90 kW	240.90 kW	240.90 kW	240.90 kW	240.90 kW	240.90 kW	240.90 kW	240.90 kW
P_{wf}	172.92 kW	172.92 kW	172.92 kW	172.92 kW	172.92 kW	172.92 kW	172.92 kW	172.92 kW
P_{loss}	1094.02 kW	921.89 kW	808.85 kW	730.51 kW	1032.05 kW	884.81 kW	779 kW	172.92 kW
η	98.834 %	98.680 %	98.250 %	96.944 %	99.008 %	98.868 %	98.509 %	97.294 %

TABLE V
VALIDATION OF THE SATURATION MODEL FOR THE EIGHT DISTINCT LOAD POINTS PRESENTED IN TABLE IV, USING (23)

Output	**#1**	**#2**	**#3**	**#4**	**#5**	**#6**	**#7**	**#8**
Measured I_f	1065.00 A	936.12 A	816.18 A	711.38 A	873.17 A	776.61 A	698.70 A	646.84 A
Calculated I_{fu}	907.99 A	794.05 A	689.23 A	597.70 A	747.18 A	657.57 A	586.96 A	541.21 A
Calculated I_f	1064.88 A	934.23 A	815.01 A	711.11 A	857.50 A	764.76 A	691.88 A	644.67 A
Deviation I_f	−0.01 %	−0.20 %	−0.14 %	−0.03 %	−1.79 %	−1.52 %	−0.97 %	−0.34 %

TABLE VI
WORKED EXAMPLE OF GENERATOR OPERATING IN SIX DISTINCT LOAD POINTS OVER A YEAR

Output	**#1**	**#2**	**#3**	**#4**	**#5**	**#6**	**Sum**
P_i	0.0 pu	0.0 pu	0.5 pu	0.5 pu	1.0 pu	1.0 pu	
Q_i	0.0 pu	0.5 pu	0.0 pu	0.5 pu	0.0 pu	0.5 pu	
Δt_i	1460 h	1460 h	1460 h	1460 h	1460 h	1460 h	8760 h
A_i	1/6	1/6	1/6	1/6	1/6	1/6	1
$P_{loss,i}$	0.006 76 pu	0.008 27 pu	0.007 57 pu	0.009 089 pu	0.009 99 pu	0.011 537 pu	
η_i	0 %	0 %	98.509 %	98.215 %	99.011 %	98.886 %	
E_i	0.00 GWh	0.00 GWh	75.19 GWh	75.19 GWh	150.38 GWh	150.38 GWh	451.14 GWh
$E_{loss,i}$	1.017 GWh	1.244 GWh	1.138 GWh	1.367 GWh	1.503 GWh	1.735 GWh	8.004 GWh

TABLE VII
FINAL OUTPUTS FROM WORKED EXAMPLE WITH SIX DISTINCT LOAD POINTS OVER A YEAR

	E	E_{loss}	$\overline{P}$	$\overline{P}_{loss}$	η_w	$\eta_w - \eta_n$	η_a	$\eta_a - \eta_n$	$\eta_a - \eta_w$
Value	451.14 GWh	8.004 GWh	0.500 00 pu	0.008 87 pu	65.766 %	−33.068 %	98.257 %	−0.577 %	+32.491 %

TABLE VIII
FINAL OUTPUTS FROM EVEN LOAD DISTRIBUTION OVER A WHOLE YEAR WITH 179851 NUMBER OF ELEMENTS (N)

	E	E_{loss}	$\overline{P}$	$\overline{P}_{loss}$	η_w	$\eta_w - \eta_n$	η_a	$\eta_a - \eta_n$	$\eta_a - \eta_w$
Value	404.927 GWh	7.248 GWh	0.448 78 pu	0.008 03 pu	95.923 %	−2.911 %	98.242 %	−0.592 %	+2.319 %

the other one (b) is a case of uniform distribution above 0.02 pu active power, in addition to being dominated by load operations mimicking a synchronous condenser operation below 0.02 pu. In Fig. 6-(b), the generator operates 60.5 % of the time in SCM mode. The overall results of this study are included in the final comparison presented in Table IX below.

For simplicity, the load operations in the even regions are equally distributed throughout the capability diagram. The evenly distributed case was studied as a function of the number of elements (N) inside the capability diagram in Fig. 7. As N is increasing, both the AAE and the WAE are shown to converge toward asymptotic values that are presented in Table VIII. A deviation between the AAE and WAE is found to be 1.43 %. The AAE and WAE behave similarly with very few elements, but the weighting of the AAE and the WAE begins to diverge with higher N. This is because more elements will now be placed closer to the boundary of the synchronous condenser operations, where the efficiency is steeply approaching zero.

TABLE IX
AAE AND THE WAE FOR THE DIFFERENT LOAD DISTRIBUTION PRESENTED IN FIGS. 10 AND 6.

Distribution	E	E_{loss}	$\overline{P}$	$\overline{P}_{loss}$	$\boldsymbol{\eta_w}$	$\boldsymbol{\eta_a}$	$\boldsymbol{\eta_a - \eta_w}$	N
Concentrated load distribution[1] (measured)	652.175 GWh	7.715 GWh	0.7354 pu	0.0087 pu	98.17 %	98.83 %	+0.67 %	8610
Uniform load distribution[2]	412.11 GWh	7.25 GWh	0.457 pu	0.0080 pu	96.84 %	98.27 %	+1.43 %	641
Synchronous condenser-dominated distribution[3]	165.98 GWh	6.82 GWh	0.1840 pu	0.0076	62.87 %	96.05 %	+33.18 %	623

[1] Elements are not discrete but measured every hour for 8610 h; [2] Operates 8760 h with equal weight for every element (Fig. 6 a); [3] Operates 8760 h with higher probability of occurance in SCM (Fig. 6 b). The WAE is 62.87 % and not lowered as much as theoretically expected since P is not set exactly to zero during the SCM operation, i.e, P was 0.004895 pu, yielding a mean SCM efficiency (η_{scm}) of 40.5354 % during 60.5 % of its operational time.

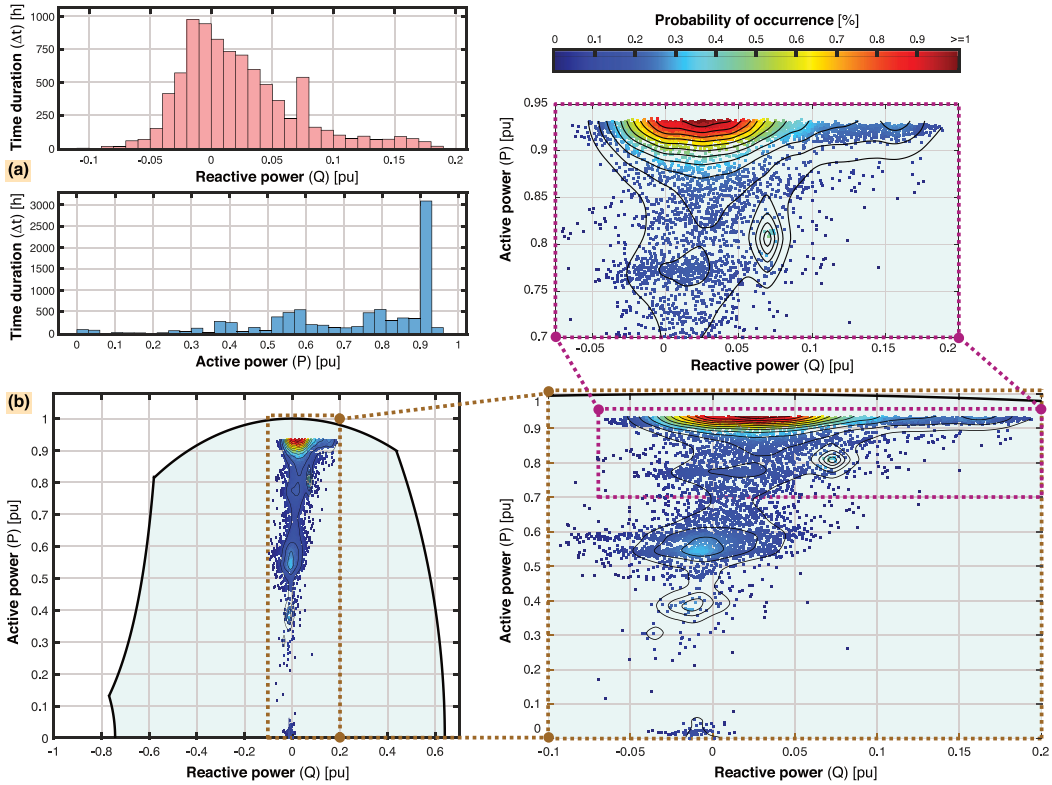

Fig. 10. Load distributions for a whole year of the studied hydropower plant (concentrated load dis.). The minimum and maximum reactive power ranges from -0.08 to 0.2 pu. The minimum and maximum active power are varying from 0 to 1 pu. The measurements were recorded every hour, starting from 06 January 2020 15:00, ending at 31 December 2020 (i.e., 8610 h in total). The generator were operated 3087 h around the vicinity of the P_{max} region. Contour lines are added to indicate the density peaks. **a)**: One-dimensional histogram of number of hours (Δt). **b)**: Two-dimensional histogram of probability of occurrence in percent (%).

D. Even Distribution With Power Constraints

The characteristics of the AAE and WAE have also been tested for even distribution with different active power constraints. First, the maximum active power threshold was ramped from 0 pu to 1 pu, which is illustrated in Fig. 8. At unity maximum power, the efficiencies are equal to what is reported in Table VIII and the asymptotic values of Fig. 7. The disparities between the AAE and the WAE are greatest at active power levels from 0 to 0.3 pu and highlights that the WAE is an insufficient model for low power levels, contrary to the AAE. However, both models have low efficiency as the threshold approaches zero.

In Fig. 9, a minimum active power threshold is ramped from 0.99 to 0 pu. In general, WAE is revealed to be a good model for load operations with a relatively high minimum active power threshold. However, as one lowers the minimum power threshold, the value converges to its uniform distribution value, as mentioned earlier, clearly deviating from the AAE.

E. Concentrated Distribution Case From On-Site Measurements

In [1], the WAE is calculated using approximated zones of load operations. In other words, the zone consist of all the exact load operations rounded up to discrete load points. This means that the histogram does not show all the distinct load operations. In Fig. 10, the exact load operations are presented in a scatter plot that highlights the density of the occurring load operations. The probability of occurrence is determined based on the proximity of the exact load points. This means that the histogram does not show the probability of an exact loading but rather the likelihood of a discrete load point occurring in a certain region.

The concentrated load distribution gathered from a year of on-site measurements provides the most similar efficiency levels, comparing the AAE and the WAE. The difference in efficiency was found to be 0.67 %. This is because, in this distribution, a lot of the load operations are concentrated around P_{max} and

operate in a relatively small area. Moreover, the generator is rarely operated in SCM. Still, $0.67\,\%$ difference is a major difference between the AEE and the WAE when considering the economic implications of this difference, if the WAE would be considered as physical. A final comparison that summarizes the findings are provided in Table IX.

VI. Conclusion

A new method to determine the overall operating efficiency of synchronous generators under intermittent operation is proposed, where the machine's magnetic saturation has been incorporated. It is shown that the proposed AAE is more effective and adaptable than the alternative WAE for all the different load distributions that were investigated. The AAE is, therefore, a necessary tool to quantify a generator's overall efficiency accurately in future operating regimes. To legitimize the results, our efficiency and loss map has been validated by eight handpicked load-point measurements. The following findings comparing the AAE and the WAE have been identified.

1) A load distribution dominated by SCM yields a difference as high as $33.18\,\%$, while an even distribution deviates by $1.43\,\%$ in their respective efficiencies;
2) A concentrated load distribution found from a full year of measurements on the studied generator revealed a discrepancy of $0.67\,\%$, which is a significant deviation considering what the operating regime would mean in terms of economic implications. E.g., designing a generator with $98.17\,\%$ compared to $98.83\,\%$ could yield a significant discrepancy in return on investment over the generators lifetime.
3) It is perceived that there is no physical relevance to the significant reduction in the WAE. This paper compares the WAE against the AAE and shows that the WAE is much more heavily influenced by the weight coefficients and by intervals of low active power.

Finally, this paper prepares for a wide spectrum of further research. The additional costs for intermittent operation of hydrogenerators should not merely be investigated in terms of losses, but also its implication on the generator's lifetime. The burden is not only influenced by the static load points, but also by the rapid transitions between them. Future work should also investigate how the loading regime could be better incorporated into the design of hydrogenerators from scratch.

Acknowledgment

The authors gratefully acknowledge the economic support from The Research Council of Norway and industry partners through Research Council's Project - "System Optimization between power producer and grid owners for more efficient system services" (SysOpt).

References

[1] E. d. C. Bortoni, R. T. Siniscalchi, S. Vaschetto, M. A. Darmani, and A. Cavagnino, "Efficiency mapping and weighted average efficiency for large hydrogenerators," *IEEE Open J. Ind. Appl.*, vol. 2, pp. 11–20, Jan. 2021.

[2] E. Agneholm *et al.*, "Report on coordination of grid codes and generator standards: Consequences of diverse grid code requirements an synchronous machine design and standards," Tech. Rep. PES-TR69, pp. 1–88, Feb. 2019. [Online]. Available: https://resourcecenter.ieee-pes.org/publications/technical-reports/PES_TR_11-18_0069.html

[3] E. C. Bortoni, M. K. I. Uemori, B. T. Araujo, J. V. Bernardes, J. J. Rocha E., and R. T. Siniscalchi, "Accurate methodology to obtain efficiency mapping of synchronous machines," in *Proc. IEEE Power Energy Soc. Gen. Meeting*, 2020, pp. 1–5.

[4] A. Nami, "Power electronics for future power grids: Drivers and challenges," in *Proc. 20th Eur. Conf. Power Electron. Appl.*, 2018, pp. P.1–P.2.

[5] J.-H. Braam, "Development, test and validation of new generator product line for current and future operational regimes," in *Proc. CIGRE*, A1-103, 2018, pp. 1–10.

[6] A. Joswig, K. Walli, and M. Baca, "Synchronous rotating equipment as backbone for renewables," in *Proc. VDE High Voltage Technol. 2018, ETG-Symp.*, 2018, pp. 1–6.

[7] J. K. Nøland, M. Leandro, A. Nysveen, and T. Øyvang, "Future operational regimes of bulk power generation in the era of global energy transition: Grid codes, challenges and open issues," in *Proc. IEEE Power Energy Soc. Gen. Meeting*, 2020, pp. 1–5.

[8] W. Tang, J. Hu, Y. Chang, and X. Kong, "Short-circuit current of grid-connected voltage source converters: Multi-timescale analysis method," in *Proc. IEEE PES GM*, 2017, pp. 1–5.

[9] T. Øyvang, J. K. Nøland, R. Sharma, G. J. Hegglid, and B. Lie, "Enhanced power capability of generator units for increased operational security using NMPC," *IEEE Trans. Power Syst.*, vol. 35, no. 2, pp. 1562–1571, Mar. 2020.

[10] C. Carounagarane, T. R. Chelliah, and D. Khare, "Analysis on thermal behavior of large hydrogenerators operating with continuous overloads," *IEEE Trans. Ind. Appl.*, vol. 56, no. 2, pp. 1293–1305, Mar./Apr. 2020.

[11] T. Tellefsen, J. van Putten, and O. Gjerde, "Norwegian hydropower: Connecting to continental europe," *IEEE Power Energy Mag.*, vol. 18, no. 5, pp. 27–35, Sep./Oct. 2020.

[12] S. Wang, J. Liu, H. Chen, R. Bo, and Y. Chen, "Modeling state transition and head-dependent efficiency curve for pumped storage hydro in look-ahead dispatch," *IEEE Trans. Power Syst.*, vol. 36, no. 6, pp. 5396–5407, Nov. 2021.

[13] W. Yang *et al.*, "Burden on hydropower units for short-term balancing of renewable power systems," *Nat. Commun.*, vol. 9, no. 1, pp. 1–12, 2018.

[14] F. Maurer and J. K. Nøland, "A rectangular end-winding model for enhanced circulating current prediction in AC machines," *IEEE Trans. Energy Convers.*, vol. 36, no. 1, pp. 291–299, Mar. 2021.

[15] J. K. Nøland, S. Nuzzo, A. Tessarolo, and E. F. Alves, "Excitation system technologies for wound-field synchronous machines: Survey of solutions and evolving trends," *IEEE Access*, vol. 7, pp. 109 699–109 718, 2019.

[16] J. C. Akiror, P. Pillay, and A. Merkhouf, "Effect of saturation on rotational flux distribution in hydro generators," *IEEE Trans. Energy Convers.*, vol. 31, no. 4, pp. 1657–1664, Dec. 2016.

[17] "Commission regulation (EU) establishing a network code on requirements for grid connection of generators (NC-RfG)," *Eur. Commission*, pp. 1–68, Apr. 2016.

[18] "NVF 2020 National guide for functional requirements in the power system," *Statnett*, pp. 1–226, Jul. 2020. [Online]. Available: https://www.statnett.no/globalassets/for-aktorer-i-kraftsystemet/systemansvaret/retningslinjer-fos/nvf-2021---nasjonal-veileder-for-funksjonskrav-i-kraftsystemet.pdf

[19] J. R. B. Jan Machowski, Z. Lubosny, and J. W. Bialek, *Power System Dynamics: Stability and Control*, 3rd ed. Chichester: Wiley, 2020.

[20] *IEEE Guide for Test Procedures for Synchronous Machines Including Acceptance and Performance Testing and Parameter Determination for Dynamic Analysis*, IEEE Standard 115-2019 (Revision of IEEE Std 115-2009), pp. 1–246, 2020.

[21] B. T. Araujo, M. S. Han, B. Kawkabani, and E. C. Bortoni, "Estimation of the armature leakage reactance using the constant excitation test," in *Proc. 22nd Int. Conf. Electr. Mach.*, 2016, pp. 313–317.

[22] T. Øyvang, J. K. Nøland, G. J. Hegglid, and B. Lie, "Online model-based thermal prediction for flexible control of an air-cooled hydrogenerator," *IEEE Trans. Ind. Electron.*, vol. 66, no. 8, pp. 6311–6320, Aug. 2019.

[23] E. da Costa Bortoni, R. T. Siniscalchi, and J. A. Jardini, "Determination of hydro generator efficiency using infrared thermal imaging techniques," *IEEE Trans. Energy Convers.*, vol. 26, no. 4, pp. 1134–1139, Dec. 2011.

Yannick Cyiza Karekezi was born in Kigali, Rwanda, in 1996. He received the M.Sc. degree in electric power engineering from the Norwegian University of Science and Technology (NTNU), Trondheim, Norway, in 2021. He is currently working toward the Ph.D. degree with the Department of Electric Power Engineering (IEL), NTNU. In addition, he is also a part-time Scientific Assistant with the Department of Electrical Engineering, Information Technology and Cybernetics, University of South-Eastern Norway (USN), Notodden, Norway. His research interests include saturation, salient-pole synchronous generators, and power system dynamics. He has been a Board Member of the IEEE Power and Energy Society (PES) Norwegian Chapter since 2021.

Thomas Øyvang (Member, IEEE) received the Ph.D. degree in process, energy and automation from the University of South–Eastern Norway (USN), Notodden, Norway, in 2018. Since January 2019, he has been an Associate Professor, and the Research and Development Manager for the Research Group Hydro Power, Transmission and Distribution with the USN. His research interests include control systems, salient-pole synchronous generators, and power system dynamics. Dr. Øyvang is a Board Member of the Norwegian Academic Committee of Publication in Technology.

Jonas Kristiansen Nøland (Member, IEEE) was born in Drammen, Norway, in 1988. He received the M.Sc. degree in electric power engineering from the Chalmers University of Technology, Gothenburg, Sweden, in 2013, and the Ph.D. degree in engineering physics from Uppsala University, Uppsala, Sweden, in 2017. Since 2018, he has been an Associate Professor with the Department of Electric Power Engineering, Norwegian University of Science and Technology, Trondheim, Norway. He is also currently an Associate Professor II with the Department of Electrical engineering, Information Technology and Cybernetics, University of South-Eastern Norway, Notodden, Norway. His research interests include excitation systems, hydrogenerators, large AC machines, and enhancing their utilization, high-power machinery for aircraft applications, hyperloop propulsion and levitation, and transportation electrification in general. He is the Editor for the IEEE TRANSACTIONS ON ENERGY CONVERSION and an Associate Editor for the IEEE TRANSACTIONS ON INDUSTRIAL ELECTRONICS.